



- 1
- 2
- 3
- 4
- 5
- 6
- 7
- 8
- 9
- 10
- 11
- 12
- 13
- 14
- 15
- 16
- 17
- 18

4

5

7

9

17



19 **Abstract**

20           The Pacific-North American (PNA) teleconnection is one of the most important climate  
21 modes in the present climate condition, and it enables climate variations in the tropical Pacific to  
22 exert significant impacts on North America. Here, we show climate simulations that the PNA  
23 teleconnection was largely distorted or broken at the Last Glacial Maximum (LGM). The  
24 distorted PNA is caused by a split of the westerly jet stream, which is ultimately forced by the  
25 thick and large Laurentide ice sheet at the LGM. Changes in the jet stream greatly alter the  
26 extratropical wave guide, distorting wave propagation from the North Pacific to North America.  
27 The distorted PNA suggests that climate variability in the tropical Pacific, notably, El Niño and  
28 Southern Oscillation (ENSO), would have little direct impact on North American climate at the  
29 LGM.

30  
31  
32  
33  
34  
35  
36  
37  
38  
39  
40  
41



## 42 **1 Introduction**

43       The Pacific-Northern-American (PNA) teleconnection is the major atmospheric  
44 teleconnection mode that links climate variations from the tropical Pacific to North America for  
45 the present-day climate state (Horel and Wallace, 1981; Wallace and Gutzler, 1981). Especially,  
46 climate variability associated with El Niño and Southern Oscillation (ENSO) exerts great  
47 impacts on the North American climate through the PNA teleconnection (Henderson and  
48 Robinson, 1994; Lau, 1997; Leathers et al., 1991; Straus and Shukla, 2002). It is well known that  
49 the PNA is largely constrained by extratropical atmospheric flows, notably, the extratropical  
50 wave guide (Held, 1983; Held et al., 2002; Hoskins and Karoly, 1981; Jin and Hoskins, 1995).  
51 Thus, changes in extratropical atmospheric flows should alter the PNA under different climate  
52 conditions.

53       It has been shown that greenhouse warming leads to a strengthening and a shift of the PNA  
54 due to altered extratropical atmospheric flows (Allan et al., 2014; Chen et al., 2017). There has  
55 also been a large body of works that demonstrated significant differences in extratropical  
56 atmospheric circulations in cold climates, notably, the Last Glacial Maximum (LGM). It was  
57 shown that during the LGM the Aleutian low pressure system was enhanced in winter, the  
58 Pacific high pressure system was weakened in summer (Yanase and Abe-Ouchi, 2007; Yanase  
59 and Abe-Ouchi, 2010), the westerly jet shifted southward (Braconnot et al., 2007; Otto-Bliesner  
60 et al., 2006), and transient waves were weakened over the North Pacific and strengthened over  
61 the North Atlantic (Justino and Peltier, 2005; Justino et al., 2005). These works suggest that the  
62 PNA could be changed for different climate regimes. Therefore, a natural question is whether the  
63 PNA is also significantly altered due to atmospheric circulation changes at the LGM.



64 The LGM occurred between 23,000 and 19,000 years ago (Clark et al., 2009; Clark and  
65 Mix, 2002). One of the most significant climatic characteristics at LGM is the maximum  
66 expansion of mid-latitude ice sheets. Extensive ice sheets grew over North America and  
67 northwestern Europe, with the Laurentide ice sheet over North America, in particular, of an ice  
68 thickness of 3 to 4 kilometers (Marshall et al., 2002). Early simulations have shown that the thick  
69 and large Laurentide ice sheet forced a split of the extratropical westerly jet stream into the  
70 northern and southern branches (Cohmap, 1988; Kutzbach and Wright, 1985; Rind, 1987), and  
71 that the jet split leads to regional climate changes over the globe, especially over North America.  
72 Proxy records showed that there were more storms and precipitation associated with the southern  
73 branch, causing high lake levels and increased woodlands in the southwestern United States  
74 (Cohmap, 1988; Kutzbach and Wright, 1985).

75 Recent modeling studies showed that the Arctic Oscillation and storm tracks at LGM  
76 differ significantly from the present (Justino and Peltier, 2005; Lamy et al., 2009; Li and Battisti,  
77 2008; Lü et al., 2010; Rivière et al., 2010), and that the Laurentide ice sheet can also influence  
78 the Southern-Hemisphere atmospheric teleconnection and climate variability over West  
79 Antarctic (Jones et al., 2018). Therefore, it is possible that changed atmospheric circulations at  
80 LGM might also significantly alter the PNA and thus climate linkage between the tropical  
81 Pacific and North America.

82 In the present paper, using climate simulation results, we show that the PNA is largely  
83 distorted or even broken by the Laurentide ice sheet at LGM, and that ENSO had little direct  
84 impact on North American climates. We will also address how the PNA is altered by the  
85 Laurentide ice sheet.

## 86 **2 Models and data**



87 The simulation results from the Paleoclimate Modeling Intercomparison Project 2 (PMIP2)  
88 (Braconnot et al., 2012; Braconnot et al., 2007) and 3 (PMIP3) (Abe-Ouchi et al., 2015) are  
89 utilized in this study. By comparing the PNA patterns in the Preindustrial condition (PIC) with  
90 LGM simulations as well as our own sensitivity simulations, the changes in the PNA pattern at  
91 LGM are identified. For comparison, we also use the NCEP/NCAR reanalysis data (Kistler et al.,  
92 2001). We shall mainly focus on the simulation results from the Community Climate System  
93 Model version 3 (CCSM3) (Collins et al., 2006; Jones et al., 2018; Otto-Bliesner et al., 2006;  
94 Yeager et al., 2006), since our sensitivity simulations are performed with the same model.

95 To understand the impact of the topography of the Northern-Hemisphere glacial ice sheets  
96 on the PNA, we performed a series of sensitivity simulations with different ice sheet thicknesses,  
97 which are 0%, 20%, 40%, 60%, 80%, 100%, and 150% of the ice sheet thickness that was used  
98 in PMIP2. Here, the case of 0% ice sheet thickness means that the thickness of the ice sheet is set  
99 to zero, but the surface albedo remains ice albedo. All other conditions remain the same as that in  
100 the LGM simulations of PMIP2. The model for the sensitivity simulations is a lower-resolution  
101 version of CCSM3 (T31), which differs from that used in PMIP2 (T42). All analyses are  
102 conducted with monthly-mean model outputs of the last 30-year simulations.

103 Following Horel and Wallace (1981) and Wallace and Gutzler (1981), the PNA  
104 teleconnection is characterized by the pointwise correlation method. The four base points that  
105 represent the centers of action are located near Hawaii (20 °N, 160 °W), North Pacific (45 °N,  
106 165 °W), Alberta (55 °N, 115 °W), and the Gulf Coast (30 °N, 85 °W), respectively. The four  
107 base points were objectively derived with teleconnectivity analysis (Sherriff-Tadano and Itoh,  
108 2013; Wallace and Gutzler, 1981). To examine whether models can reasonably simulate the  
109 PNA in PIC simulations and whether the PNA pathway is altered in LGM simulations, we



loosely define a circular region around each of the centers of North Pacific, North America and the Gulf Coast (the base point is near Hawaii), with a radius of 10 degrees. For PIC simulations, if a model cannot generate statistically significant correlations (coefficients greater than 0.35) within the circular regions, the model is considered to have poor performance in simulating PNA. For these models with good performance in simulating PNA their PIC simulations, if their LGM simulations shows absence of significant correlations in the three circular regions, the PNA pathway is considered to be distorted or broken at LGM. Because the PNA is most active in DJF, our analysis below will mainly focus on the December-January-February (DJF) season.

### 3 Results

Fig. 1 shows one-point correlation maps of 500 hPa geopotential heights in DJF, with the base point near Hawaii. The correlation maps in Figs. 1a and 1b exhibit similar wave-train patterns, with centers of positive and negative correlations extending from Hawaii to North Pacific, Alberta, and finally to the Gulf Coast, respectively. Hence, the present-day PNA is reproduced reasonably well in CCSM3. In contrast, this PNA pattern is altered dramatically in the LGM simulation of CCSM3 (Fig. 1c). The negative correlation over North Pacific is reduced, and the center of positive correlation is rather weak and shifted to the Arctic. The most striking feature in Fig. 1c is that the center of negative correlation near the Gulf Coast completely disappears. The results in Fig. 1 indicate that the PNA teleconnection is largely distorted at LGM. This is the most important point of the present paper.

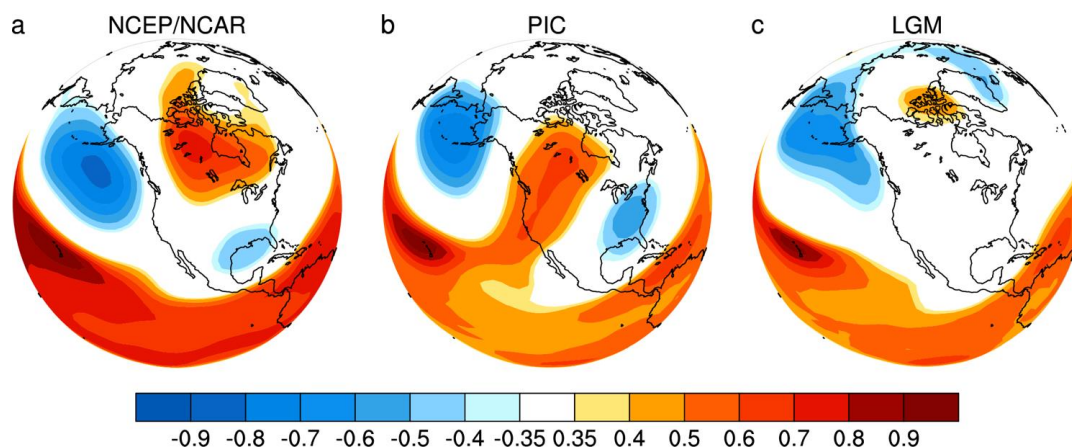


**Fig. 1.** One-point correlation maps of 500 hPa geopotential heights in DJF in NCEP/NCAR reanalysis and PMIP2 CCSM3 simulations. (a) NCEP/NCAR, (b) PIC, and (c) LGM. The base point is near Hawaii. The correlation coefficient of 0.35 corresponds to the 95% confidence level for 30-year correlations.

This distorted PNA at LGM can also be seen from correlation maps for the other three base points. When the base point is located over North Pacific (Fig. S1c), the center of positive correlation over North America is shifted to northern Canada. For the base point over North America (Fig. S1f), the negative correlations over North Pacific and the Gulf Coast are all largely reduced, and the center of positive correlation near Hawaii disappears. This result indicates a disconnection between North America and the tropical Pacific. For the base point near the Gulf Coast (Fig. S1i), a wave train is established from North Pacific to the Gulf Coast, while the center of positive correlation over North America is largely reduced, and the center of positive correlation near Hawaii is absent.

The PNA teleconnection at LGM is even completely broken in other PMIP2 models. There are seven PMIP2 models that have simulations available online. According to our definition, CCSM3, ECBILTCLIO, HadCM3M2, and CNRM-CM33 can reasonably reproduce the PNA in their PIC simulations (Fig. 1b and Figs. S2a-c), whereas IPSL-CM4-V1-MR, FGOALS-1.0g,



147 and MIROC3.2 have poor performance. In LGM simulations, the center of negative correlation  
 148 over North Pacific still exists in ECBILTCLIO, HadCM3M2, and CNRM-CM33 (Figs. S2d-f),  
 149 although they all shift away from the North Pacific base point and are largely reduced. However,  
 150 the center of positive correlation over North America completely disappears in these plots.  
 151 Moreover, the center of negative correlation near the Gulf Coast also disappears in the three  
 152 models.

153 PMIP3 simulations are also used to demonstrate the changes in the PNA teleconnection at  
 154 LGM. There are eight PMIP3 models that have LGM simulations available online. Again,  
 155 according to our definition, CCSM4, MRI-CGCM3, and MIROC-ESM can reasonably reproduce  
 156 the PNA in their PIC simulations (Figs. S3a-c). The LGM simulations of CCSM4 and MRI-  
 157 CGCM3 show the absence of the center of positive correlation over North America (Figs. S3d  
 158 and e). The center of positive correlation in MIROC-ESM is weak and biased toward the Arctic  
 159 (Fig. S3f). The center of negative correlation near the Gulf Coast is absent in MRI-CGCM3 and  
 160 MIROC-ESM. Although there is a negative center in CCSM4 (Fig. S3d), it is more like a result  
 161 of the subtropical wave train, rather than a part of PNA. Thus, the LGM simulations in PMIP3  
 162 models demonstrate that the PNA is either distorted or completely broken.

163 Fig. 2 illustrates PNA responses to different ice sheet thicknesses in sensitivity simulations.  
 164 The PNA pattern remains for ice sheet thicknesses no more than 60% of that in PMIP2 (Figs. 2a-  
 165 d). In contrast, the PNA is distorted as ice sheet thickness is increased to 80%. The center of  
 166 positive correlation is shifted to the Arctic, and the center of negative correlation near the Gulf  
 167 Coast disappears (Fig. 2e). As ice sheet thickness is further increased to 100 % and 150% (Figs.  
 168 2f-g), the center of positive correlation over North America disappears. Again, the center of  
 169 negative correlation is more like a part of the subtropical wave train. These results of sensitivity





simulations suggest that the PNA is distorted or even broken as the Laurentide ice sheet is sufficiently thick.

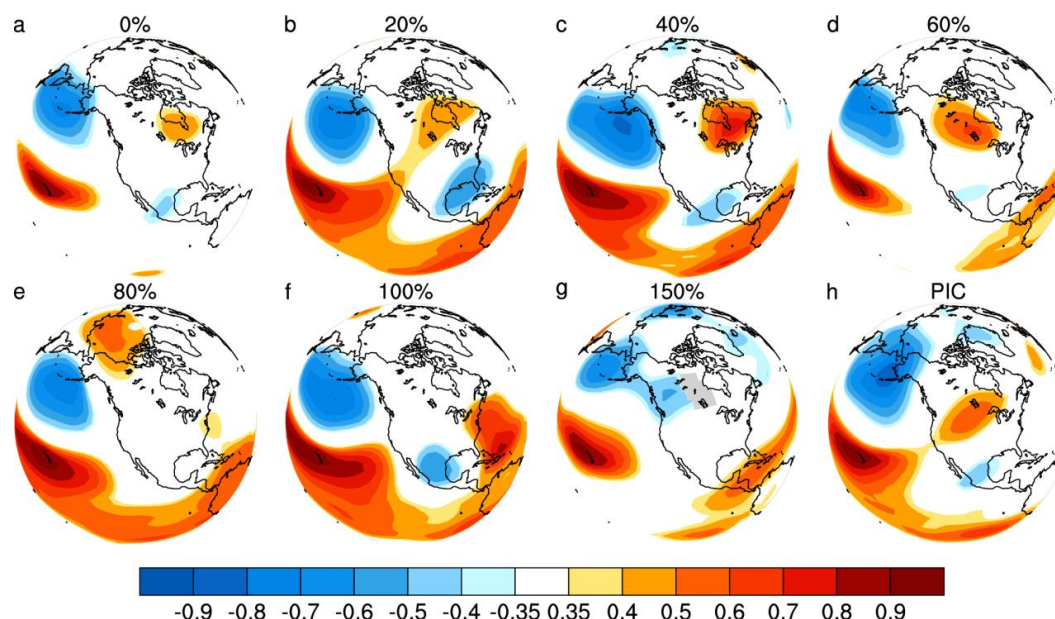
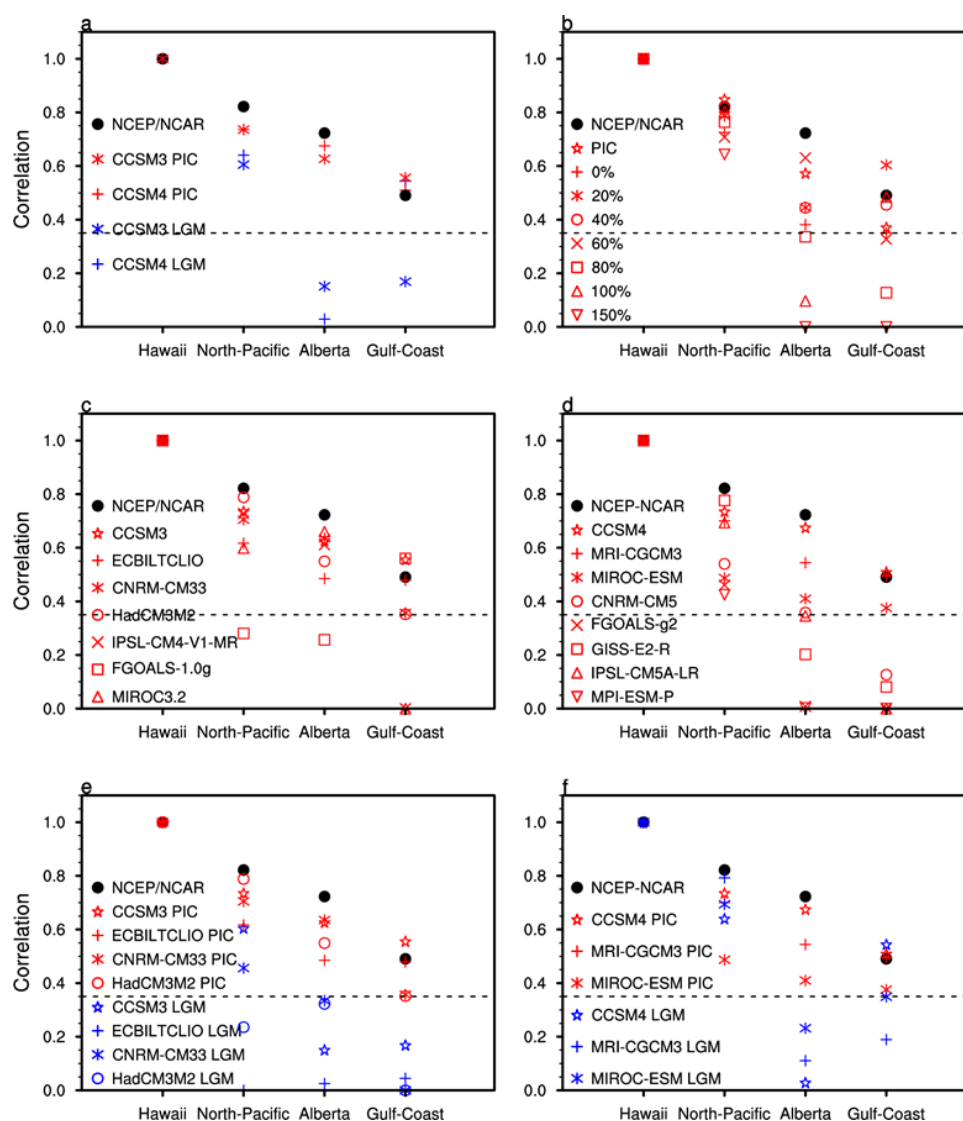


**Fig. 2.** One-point correlation maps of 500 hPa geopotential heights in DJF in sensitivity simulations, with different ice sheet thicknesses. The base point is near Hawaii. (a) 0%, (b) 20%. (c) 40%, (d) 60%, (e) 80%, (f) 100%, (g) 150%, and (h) PIC. The correlation coefficient of 0.35 corresponds to the 95% confidence level for 30-year correlations.

Fig. 3 summarizes correlation coefficients around the four base points for PMIP2, PMIP3, and our sensitivity simulations, according to our definition above. In Fig. 3a, both CCSM3 and CCSM4 show statistically significant correlations at all the four points in the PIC simulations. In contrast, they all demonstrate insignificant correlations near Alberta in LGM simulations. The significant correlation of CCSM4 LGM simulation near the Gulf coast is a result of subtropical wave train (Fig. S3d), as mentioned above. In Fig. 3b, the correlation coefficient near Alberta becomes less significant as ice sheet thickness reaches 80%. Correlation coefficients at the Gulf coast are insignificant for 80% and 150% ice sheet thickness. The



185 significant correlation for 100% ice sheet thickness is a result of subtropical wave train, as shown  
 186 in Fig. 2f.



187

188 **Fig. 3.** Correlation coefficients at the four PNA action centers in PIC and LGM simulations for  
 189 PMIP2 and PMIP3 models, with the base point near Hawaii. The negative values over Alberta and  
 190 the Gulf Coast are reversed to positive. The dashed lines correspond to 0.35, which represent the  
 191 95% confidence level. (a) CCSM3 and CCSM4, (b) sensitivity simulations, (c) PIC simulations of  
 192 PMIP2 models, (d) PIC simulations of PMIP3 models, (e) comparison of LGM with PIC



193 simulations for PMIP2 good performance models, and (f) comparison of LGM with PIC  
 194 simulations for PMIP3 good performance models.

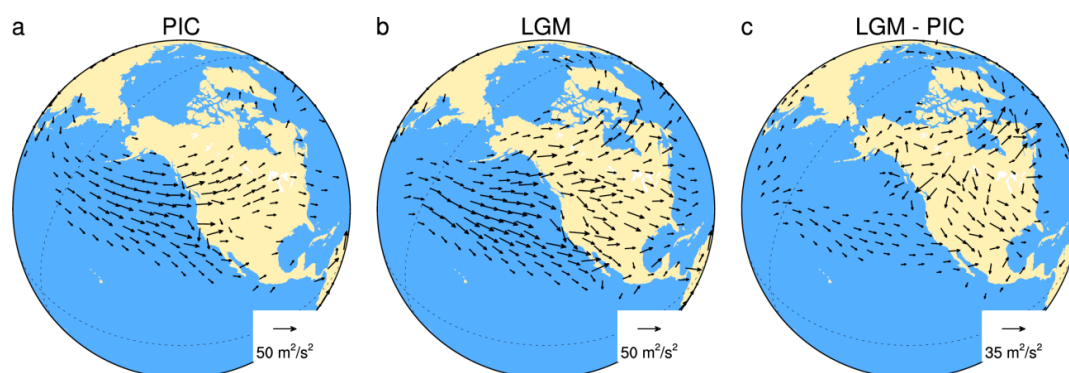
195

196 Figs. 3c and d shows that most PMIP2 and PMIP3 models are able to reproduce the  
 197 center of negative correlations over the North Pacific in their PIC simulations, except for  
 198 FGOAL-1.0g, IPSL-CN4-V1-MR, and MIROC3.2. FGOAL-1.0g that generates insignificant  
 199 correlations at either North Pacific or Alberta. CNRM-CM33 and MIROC3.2 cannot generate  
 200 significant correlations near the Gulf coast. Fig. 3d shows that CCSM4, MRI-CGCM3, and  
 201 MIROC-ESM are able to reproduce significant correlations at all four points in their PIC  
 202 simulations, whereas the other 5 models have insignificant correlations at either Albert or the  
 203 Gulf Coast. Figs. 3e and f show that PMIP2 and PMIP3 models, which have good performance  
 204 in simulating the PNA teleconnection in PIC simulations, all cannot reproduce significant  
 205 positive correlations at Alberta or even negative correlations near the Gulf coast. These results  
 206 all suggest that the PNA was distorted or broken at LGM.

207 Because the PNA pattern is characterized by a quasi-stationary wave train from the  
 208 tropical Pacific to North America, the above simulation results suggest that the PNA wave-train  
 209 propagation is largely altered at LGM. This can be confirmed by activity fluxes of stationary  
 210 waves (Fig. 4), which represents the propagation direction of stationary waves (Plumb, 1985). At  
 211 present, the wave activity fluxes have two branches for wave propagation from the North Pacific  
 212 toward North America (Fig. 4a). The major branch propagates northeastward, forming the PNA  
 213 teleconnection, while the minor branch propagates southeastward. At LGM, however, wave  
 214 propagation is altered drastically. Wave propagation is deflected toward the subtropics (Figs. 4b  
 215 and c). This is consistent with the correlation map in Fig. S1i that shows a wave train from North



216 Pacific to the Gulf Coast. Therefore, the distorted or broken PNA at LGM is mainly due to the  
 217 deflection of wave propagation toward the southeast.



218  
 219 **Fig. 4.** Stationary wave activity fluxes in PMIP2 CCSM3 simulations at 500 hPa. (a) PIC, (b)  
 220 LGM, and (c) LGM – PIC. Length scales of wave activity vectors are marked in plots. Wave  
 221 activity vectors are plotted as their length scales are greater than  $12 \text{ m}^2 \text{ s}^{-2}$  in plots (a) and (b) and  
 222  $6.5 \text{ m}^2 \text{ s}^{-2}$  in plot (c). Here, stationary wave activity fluxes are calculated with monthly-mean  
 223 data.

224 Wave propagation is oriented by the extratropical wave guide, which in turn is  
 225 determined by extratropical zonal flows (Hoskins and Karoly, 1981; Jin and Hoskins, 1995).  
 226 Therefore, the deflection of stationary wave propagation at LGM is caused due to changes in  
 227 extratropical zonal flows. A comparison of zonal winds between PIC and LGM simulations  
 228 shows several major differences (Figs. 5a vs. 5b). First, the zonal jet stream is much stronger at  
 229 LGM than at present. Second, the jet is shifted equatorward at LGM, and the jet is turned  
 230 southeastward as it approaches the North American continent, in contrast to the northeast  
 231 orientation at present. Third, similar to that in early studies (Cohmap, 1988; Kutzbach and  
 232 Wright, 1985; Rind, 1987), the jet splits over North America with the much stronger branch  
 233 located in the subtropics, leaving the much weaker branch over northern Canada. These features  
 234 can be seen more clearly in differences of zonal winds between LGM and PIC simulations (Fig.  
 235 5c).

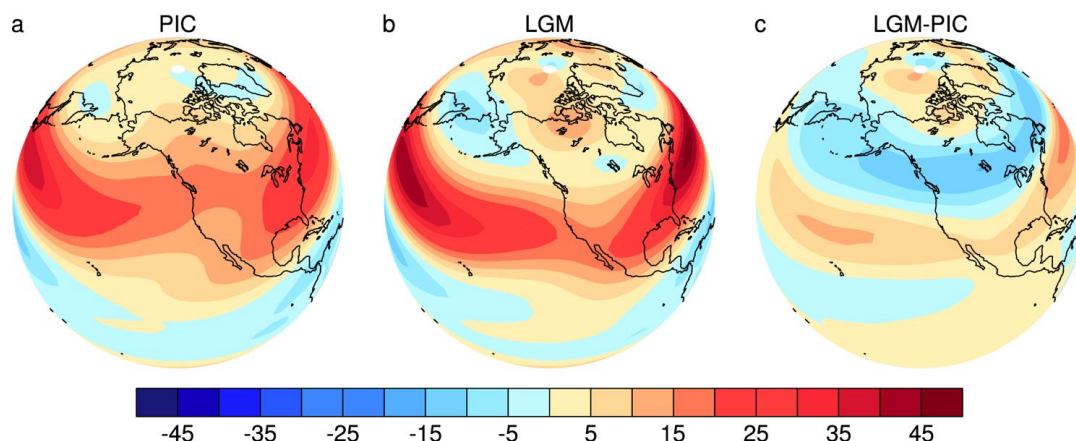


**Fig. 5.** Maps of 500 hPa zonal winds in DJF in PMIP2 CCSM3 simulations. (a) PIC, (b) LGM, and (c) LGM – PIC. Color interval:  $5 \text{ m s}^{-1}$ .

Differences of zonal winds over North American can also be illustrated with the vertical cross-sections along  $100^\circ \text{W}$  (Fig. 6). The single subtropical westerly jet in the PIC simulation (Fig. 6b) is split into two jets at LGM (Fig. 6c): a subtropical jet at  $30^\circ \text{N}$  and 200 hPa, and a subpolar jet at  $63^\circ \text{N}$  and between 400 and 300 hPa. The subtropical jet is intensified to a maximum wind speed of  $40 \text{ m s}^{-1}$  and is located at a lower latitude, and it is much stronger than that in the PIC simulation ( $\sim 30 \text{ m s}^{-1}$ ). The subpolar jet is much weaker, with a maximum speed of about  $12 \text{ m s}^{-1}$ . The differences in zonal winds are associated with different thermal structures between LGM and PIC simulations. Comparison of Figs. 6f with 6e shows that latitudinal temperature gradients in the subtropics are sharper at LGM than at present. Thus, the stronger subtropical jet is associated with the sharper temperature gradient.

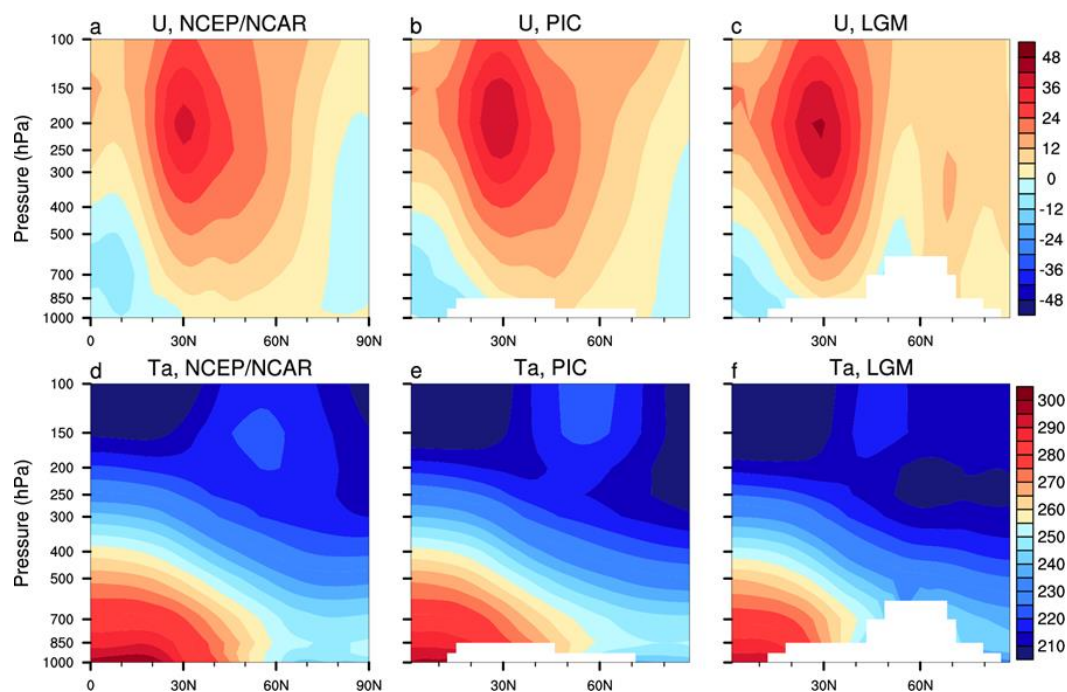


**Fig. 6.** Vertical cross sections of DJF zonal winds and air temperatures along the longitude of 100°W in the NCEP/NCAR reanalysis and PMIP2 CCSM3 simulations. Top panels: zonal winds, and bottom panels: air temperatures. Left panels: NCEP/NCAR, middle panels: PIC, and right panels: LGM. Zonal-wind unit is ms<sup>-1</sup>, and temperature unit is K.

The jet split and the equatorward shift of the major jet branch are caused by the orographic forcing of the large and thick Laurentide ice sheet. Fig. S4 shows how the westerly jet responds to the ice sheet thickness in the sensitivity simulations. In the case with 0% ice sheet thickness, there is only a single jet in the subtropics (Fig. S4a), almost the same as that in the PIC simulation. As ice sheet thickness is increased, the jet is strengthened and shows equatorward shift. Significant jet split occurs as ice sheet thickness reaches 80% (Fig. S4e). It is why the distortion of the PNA occurs as ice sheet thickness reaches 80%. As the ice sheet thickness is increased to 100% and 150%, the jet split becomes more significant, and easterly winds begin to develop over the ice sheet.





265 Note that the orographic forcing is further reinforced by the thermal forcing of the large ice  
266 sheet (Liakka, 2012). The high albedo of the ice sheet causes cold air aloft, resulting in sharper  
267 latitudinal temperature gradients in the subtropics at LGM. Thus, this enhanced temperature  
268 gradient causes a stronger subtropical jet through the thermal wind relation. Our sensitivity  
269 simulations also show that subtropical temperature gradients become sharper with increasing ice  
270 sheet thicknesses.

271 The split of the westerly jet act as wave guides to orient wave propagation, as shown in Fig.  
272 4. The major path of wave propagation is associated with the major jet branch. Both Figs. S1c  
273 and S1i all show that a southern wave train is established along the southern jet branch from  
274 North Pacific sweeping across the southern US. This wave train would lead to more storms and  
275 precipitation in the American Southwest, consistent with proxy records and previous modeling  
276 studies (Cohmap, 1988). The minor path of wave propagation toward the Arctic is along with the  
277 northern branch (Fig. 1c), but of a much reduced strength. As such, a southern wave guide is  
278 established along the subtropical jet, while the northern wave guide is either distorted toward the  
279 Arctic or completely broken.

280 Our sensitivity simulations demonstrate dramatic changes in the PNA wave train between  
281 80% and 100% ice sheet thicknesses (Fig. 2e vs. Fig. 2f). The dramatic changes are associated  
282 with the occurrence of easterly winds over the Laurentide ice sheet. For the case of 80% ice sheet  
283 thickness, westerly winds remain between the two jet streams. In contrast, easterly winds appear  
284 over the ice sheet as the ice sheet thickness is increased to 100%. The zero-wind line between  
285 easterly and westerly winds acts as the critical layer to reflect stationary waves (Held, 1983).  
286 This can be addressed with calculations of stationary wavenumbers (Fig. 7). The orange-red  
287 shading indicates the areas where stationary waves can propagate, while the shallow-blue



shading indicates the areas with imaginary wavenumbers, in which propagation of stationary waves is prohibited. These shallow-blue areas are associated with the easterly winds. When the ice sheet thickness is 60% (Fig. 7a), North Pacific and North America are dominated with positive wavenumbers, and the PNA remains. For 80% ice sheet thickness, imaginary wavenumbers occur in Northeast Pacific and North America (Fig. 7b), and it forces the PNA wave train distorted toward the Arctic. For 100% ice sheet thickness, the subpolar region is dominated with imaginary wavenumbers (Fig. 7c). It causes stationary waves reflected southeastward, leading to the establishment of the southern wave train and the breaking up of the northern wave train.

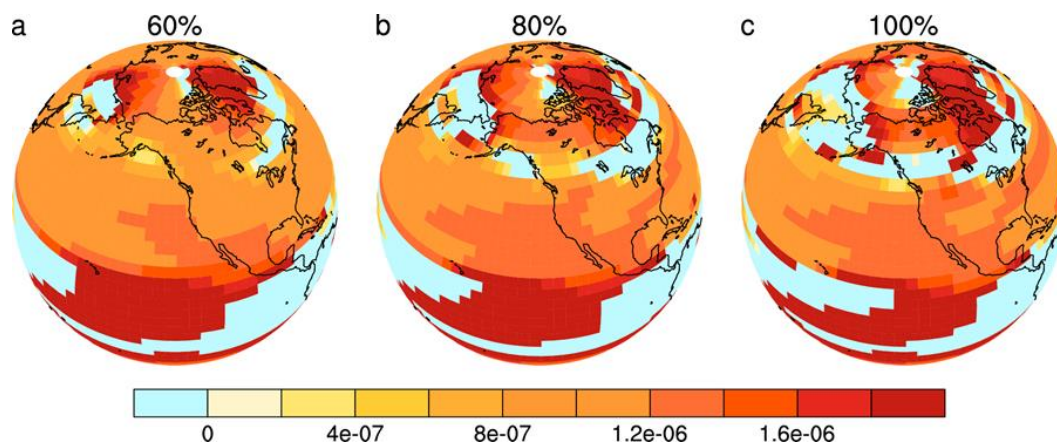


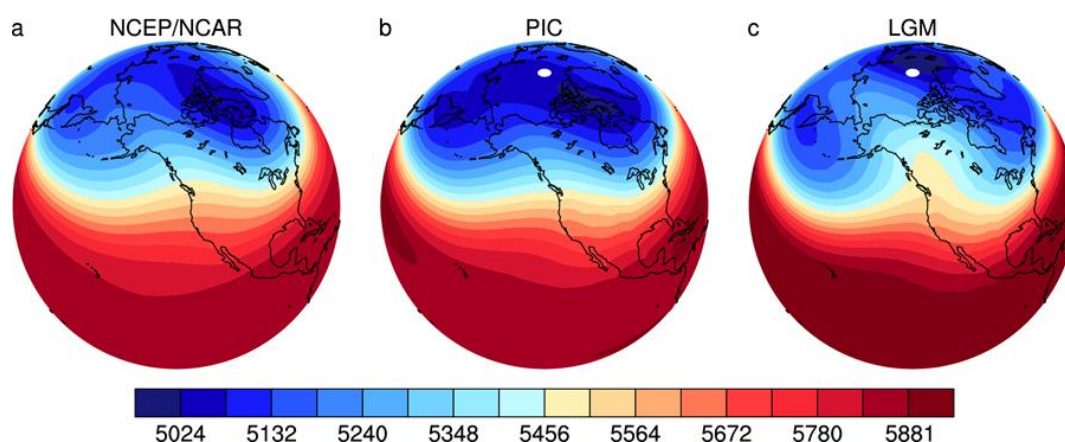
**Fig. 7.** Distributions of stationary wavenumbers for different ice sheet thicknesses in sensitivity simulations in DJF. (a) 60%, (b) 80%, and (c) 100%. Color interval is  $0.2 \times 10^{-7} \text{ m}^{-1}$ . The shallow-blue areas have imaginary wavenumbers.

The occurrence of easterly winds can be further illustrated with the geopotential heights at 500 hPa (Fig. 8). In both NCEP/NCAR reanalysis and the PIC simulation, there is only a weak ridge along the west coast of North America (Figs. 8a and b). In contrast, the ridge at LGM is largely enhanced and shows northwestern tilting (Fig. 8c). It is this strong ridge that leads to





306 altered zonal flows. The major branch moves equatorward, and the minor branch flows around  
 307 the ridge northward, resulting in the formation of easterly winds over the ice sheet and North  
 308 Pacific. It also can be seen in the sensitivity simulations that the west-coast ridge increases with  
 309 increasing ice sheet thickness (Fig. S5).



311 **Fig. 8.** Climatological mean 500 hPa geopotential heights in DJF in NCEP/NCAR reanalysis and  
 312 PMIP2 CCSM3 simulations. (a) NCEP/NCAR, (b) PIC, and (c) LGM. The unit is meter.

314 The distorted or broken PNA teleconnection at LGM suggests a disconnection of climate  
 315 variability from the tropical Pacific to the North American continent, such that ENSO would  
 316 have little direct influence on North American climates. Fig. 9 shows regression maps of surface  
 317 air temperatures (SATs) on the Nino3.4 index in DJF. At present, the remote ENSO impacts on  
 318 North American SATs through the PNA teleconnection can be identified clearly (Figs. 9a and  
 319 9b), which is characterized by an anomalously warm climate over the northwestern North  
 320 America and an anomalously cold climate over the southeastern United State. However, there are  
 321 no significant regressions of SATs over North America at LGM (Fig. 9c), except for the positive  
 322 values near the east coast.

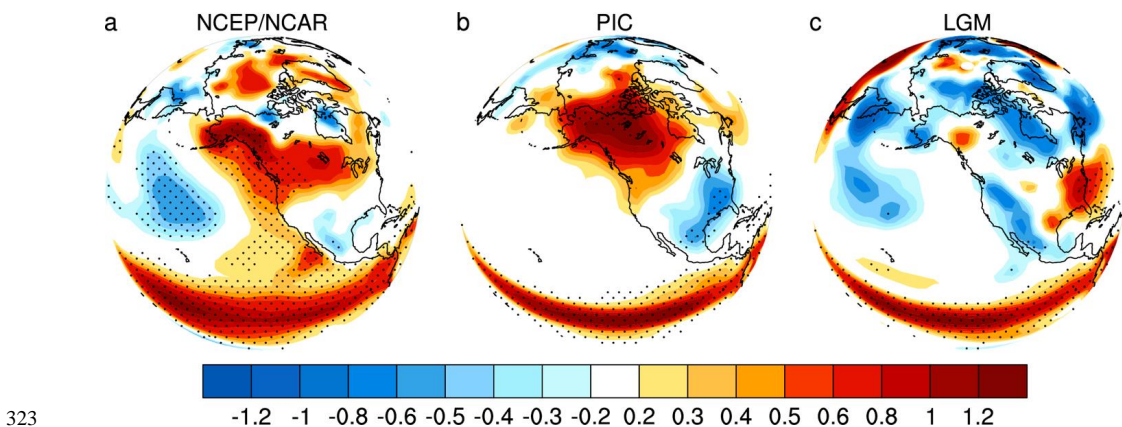


**Fig. 9.** DJF SAT regressions on the Nino3.4 index in NCEP/NCAR reanalysis and PMIP2 CCSM3 simulations. (a) NCEP/NCAR reanalysis, (b) PIC, and (c) LGM. The regression value of 0.21 corresponds to the 95% confidence level for 30-year regressions.

At present, ENSO also has important influences on North American precipitation. Similar features can also be seen from regression maps of precipitation (Fig. 10). Fig. 10a shows precipitation regression on the Nino3.4 index in the PIC simulation. The wave train pattern of precipitation is clearly shown in the plot. However, the wave train of precipitation is absent in the LGM simulations (Fig. 10b).

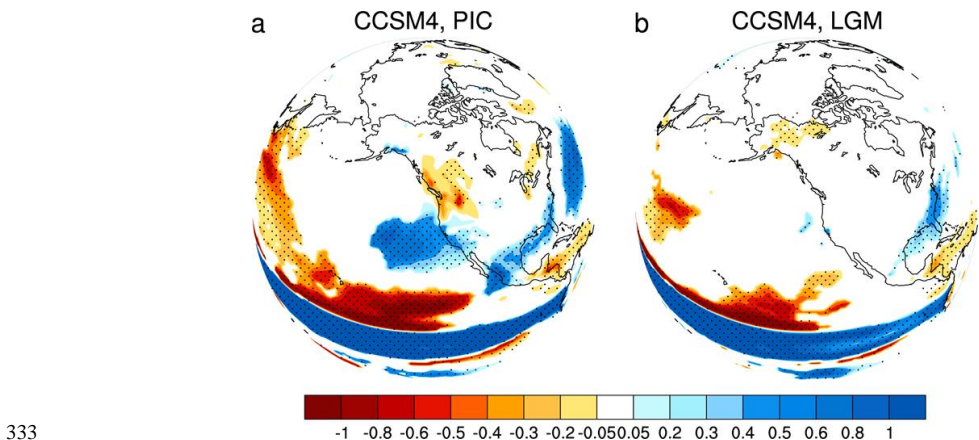


**Fig. 10.** Precipitation regressions on the Nino3.4 index in the CCSM4 PMIP3 simulations. (a) PIC, and (b) LGM. Dotted areas indicate significant regressions for the 95% confidence level for 30-year regressions.



337

#### 338 **4 Conclusions and Discussions**

339         We have showed in climate simulations that the large and thick Laurentide ice sheet at  
340 LGM forced jet split and the formation of easterly winds over North America. It consequently  
341 causes altered wave guides and distorted or broken PNA. This result suggests that ENSO would  
342 not have little direct influence on North American climates at LGM. Our study provides a  
343 dynamic framework to understand the PNA teleconnection not only at LGM but also in other  
344 glacial periods. This understanding may help us interpreting proxy records in the past. For  
345 example, a previous study on varve record in New England linked the change of the intensity of  
346 interannual variability in the northeastern US during the early glacial period to the change of  
347 ENSO intensity (Rittenour et al., 2000). Our study suggests that this interannual variability is  
348 unlikely to be caused by the climate variability from the tropical Pacific, because of the distorted  
349 or broken PNA teleconnection; instead, it reflects mainly the change of local climate variability  
350 (Liu et al., 2014). Much further work is needed in developing proxy records of high temporal  
351 resolutions to identify the PNA change in paleoclimate records.

352

#### 353 **Acknowledgements**

354         This work is supported by the National Natural Science Foundation of China under grants  
355 41888101, 41761144072, and 41630527.



## References

- Abe-Ouchi, A., Saito, F., Kageyama, M., Braconnot, P., Harrison, S. P., Lambeck, K., Otto-  
 Bliesner, B. L., Peltier, W. R., Tarasov, L., Peterschmitt, J. Y., and Takahashi, K.: Ice-sheet  
 configuration in the CMIP5/PMIP3 Last Glacial Maximum experiments, *Geosci. Model*  
*Dev.*, 8, 3621-3637, 2015.
- Allan, A. M., Hostetler, S. W., and Alder, J. R.: Analysis of the present and future winter Pacific-  
 North American teleconnection in the ECHAM5 global and RegCM3 regional climate  
 models, *Climate Dynamics*, 42, 1671-1682, 2014.
- Braconnot, P., Harrison, S. P., Kageyama, M., Bartlein, P. J., Masson-Delmotte, V., Abe-Ouchi,  
 A., Otto-Bliesner, B., and Zhao, Y.: Evaluation of climate models using palaeoclimatic data,  
*Nature Climate Change*, 2, 417, 2012.
- Braconnot, P., Otto-Bliesner, B., Harrison, S., Joussaume, S., Peterchmitt, J. Y., Abe-Ouchi, A.,  
 Crucifix, M., Driesschaert, E., Fichefet, T., Hewitt, C. D., Kageyama, M., Kitoh, A., La n é  
 A., Loutre, M. F., Marti, O., Merkel, U., Ramstein, G., Valdes, P., Weber, S. L., Yu, Y., and  
 Zhao, Y.: Results of PMIP2 coupled simulations of the Mid-Holocene and Last Glacial  
 Maximum – Part 1: experiments and large-scale features, *Clim. Past*, 3, 261-277, 2007.
- Chen, Z., Gan, B., Wu, L., and Jia, F.: Pacific-North American teleconnection and North Pacific  
 Oscillation: historical simulation and future projection in CMIP5 models, *Climate*  
*Dynamics*, doi: 10.1007/s00382-017-3881-9, 2017. 2017.
- Clark, P. U., Dyke, A. S., Shakun, J. D., Carlson, A. E., Clark, J., Wohlfarth, B., Mitrovica, J. X.,  
 Hostetler, S. W., and McCabe, A. M.: The Last Glacial Maximum, *Science*, 325, 710-714,  
 2009.



- 378 Clark, P. U. and Mix, A. C.: Ice sheets and sea level of the Last Glacial Maximum, Quaternary  
 379 Science Reviews, 21, 1-7, 2002.
- 380 Cohmap, M.: Climatic Changes of the Last 18,000 Years: Observations and Model Simulations,  
 381 Science, 241, 1043-1052, 1988.
- 382 Collins, W. D., Bitz, C. M., Blackmon, M. L., Bonan, G. B., Bretherton, C. S., Carton, J. A.,  
 383 Chang, P., Doney, S. C., Hack, J. J., Henderson, T. B., Kiehl, J. T., Large, W. G., McKenna,  
 384 D. S., Santer, B. D., and Smith, R. D.: The Community Climate System Model Version 3  
 385 (CCSM3), Journal of Climate, 19, 2122-2143, 2006.
- 386 Held, I. M.: Stationary and Quasi-stationary Eddies in the Extratropical Troposphere: Theory. In:  
 387 Large-scale Dynamical Processes in the Atmosphere, B. J. Hoskins and Pearce, R. P. (Eds.),  
 388 Academic Press, 1983.
- 389 Held, I. M., Ting, M., and Wang, H.: Northern Winter Stationary Waves: Theory and Modeling,  
 390 Journal of Climate, 15, 2125-2144, 2002.
- 391 Henderson, K. G. and Robinson, P. J.: Relationships between the pacific/north american  
 392 teleconnection patterns and precipitation events in the south - eastern USA, International  
 393 Journal of Climatology, 14, 307-323, 1994.
- 394 Horel, J. D. and Wallace, J. M.: Planetary-Scale Atmospheric Phenomena Associated with the  
 395 Southern Oscillation, Monthly Weather Review, 109, 813-829, 1981.
- 396 Hoskins, B. J. and Karoly, D. J.: The Steady Linear Response of a Spherical Atmosphere to  
 397 Thermal and Orographic Forcing, Journal of the Atmospheric Sciences, 38, 1179-1196,  
 398 1981.
- 399 Jin, F. and Hoskins, B. J.: The Direct Response to Tropical Heating in a Baroclinic Atmosphere,  
 400 Journal of the Atmospheric Sciences, 52, 307-319, 1995.



- 401 Jones, T. R., Roberts, W. H. G., Steig, E. J., Cuffey, K. M., Markle, B. R., and White, J. W. C.:  
 402 Southern Hemisphere climate variability forced by Northern Hemisphere ice-sheet  
 403 topography, *Nature*, 554, 351, 2018.
- 404 Justino, F. and Peltier, W. R.: The glacial North Atlantic Oscillation, *Geophysical Research*  
 405 *Letters*, 32, 2005.
- 406 Justino, F., Timmermann, A., Merkel, U., and Souza, E. P.: Synoptic Reorganization of  
 407 Atmospheric Flow during the Last Glacial Maximum, *Journal of Climate*, 18, 2826-2846,  
 408 2005.
- 409 Kistler, R., Kalnay, E., Collins, W., Saha, S., White, G., Woollen, J., Chelliah, M., Ebisuzaki,  
 410 W., Kanamitsu, M., Kousky, V., van den Dool, H., Jenne, R., and Fiorino, M.: The NCEP-  
 411 NCAR 50-year reanalysis: Monthly means CD-ROM and documentation, *B Am Meteorol*  
 412 *Soc*, 82, 247-267, 2001.
- 413 Kutzbach, J. E. and Wright, H. E.: Simulation of the climate of 18,000 years BP: Results for the  
 414 North American/North Atlantic/European sector and comparison with the geologic record of  
 415 North America, *Quaternary Science Reviews*, 4, 147-187, 1985.
- 416 Lamy, A., Kageyama, M., Salas-Munoz, D., Voldoire, A., Rivière, G., Ramstein, G., Planton, S.,  
 417 Tyteca, S., and Peterschmitt, J. Y.: Northern hemisphere storm tracks during the last glacial  
 418 maximum in the PMIP2 ocean-atmosphere coupled models: energetic study, seasonal cycle,  
 419 precipitation, *Climate Dynamics*, 32, 593-614, 2009.
- 420 Lau, N.-C.: Interactions between Global SST Anomalies and the Midlatitude Atmospheric  
 421 Circulation, *B Am Meteorol Soc*, 78, 21-34, 1997.



- 422 Leathers, D. J., Yarnal, B., and Palecki, M. A.: The Pacific/North American Teleconnection  
 423 Pattern and United States Climate. Part I: Regional Temperature and Precipitation  
 424 Associations, *Journal of Climate*, 4, 517-528, 1991.
- 425 Li, C. and Battisti, D. S.: Reduced Atlantic Storminess during Last Glacial Maximum: Evidence  
 426 from a Coupled Climate Model, *Journal of Climate*, 21, 3561-3579, 2008.
- 427 Liakka, J.: Interactions between topographically and thermally forced stationary waves:  
 428 implications for ice-sheet evolution, *Tellus A: Dynamic Meteorology and Oceanography*,  
 429 64, 11088, 2012.
- 430 Liu, Z., Lu, Z., Wen, X., Otto-Bliesner, B. L., Timmermann, A., and Cobb, K. M.: Evolution and  
 431 forcing mechanisms of El Niño over the past 21,000 years, *Nature*, 515, 550, 2014.
- 432 Lü J.-M., Kim, S.-J., Abe-Ouchi, A., Yu, Y., and Ohgaito, R.: Arctic Oscillation during the Mid-  
 433 Holocene and Last Glacial Maximum from PMIP2 Coupled Model Simulations, *Journal of*  
 434 *Climate*, 23, 3792-3813, 2010.
- 435 Marshall, S. J., James, T. S., and Clarke, G. K.: North American ice sheet reconstructions at the  
 436 Last Glacial Maximum, *Quaternary Science Reviews*, 21, 175-192, 2002.
- 437 Otto-Bliesner, B. L., Brady, E. C., Clauzet, G., Tomas, R., Levis, S., and Kothavala, Z.: Last  
 438 Glacial Maximum and Holocene Climate in CCSM3, *Journal of Climate*, 19, 2526-2544,  
 439 2006.
- 440 Plumb, R. A.: On the Three-Dimensional Propagation of Stationary Waves, *Journal of the*  
 441 *Atmospheric Sciences*, 42, 217-229, 1985.
- 442 Rind, D.: Components of the ice age circulation, *Journal of Geophysical Research: Atmospheres*,  
 443 92, 4241-4281, 1987.



- 444 Rittenour, T. M., Brigham-Grette, J., and Mann, M. E.: El Niño-Like Climate Teleconnections in  
 445 New England During the Late Pleistocene, *Science*, 288, 1039-1042, 2000.
- 446 Rivière, G., Lapeyre, G., Salas-Molina, D., and Kageyama, M.: Links between Rossby  
 447 Wave Breaking and the North Atlantic Oscillation–Arctic Oscillation in Present-Day and  
 448 Last Glacial Maximum Climate Simulations, *Journal of Climate*, 23, 2987-3008, 2010.
- 449 Sherriff-Tadano, S. and Itoh, H.: Teleconnection Patterns Appearing in the Streamfunction Field,  
 450 *SOLA*, 9, 115-119, 2013.
- 451 Straus, D. M. and Shukla, J.: Does ENSO Force the PNA?, *Journal of Climate*, 15, 2340-2358,  
 452 2002.
- 453 Wallace, J. M. and Gutzler, D. S.: Teleconnections in the Geopotential Height Field during the  
 454 Northern Hemisphere Winter, *Monthly Weather Review*, 109, 784-812, 1981.
- 455 Yanase, W. and Abe-Ouchi, A.: The LGM surface climate and atmospheric circulation over East  
 456 Asia and the North Pacific in the PMIP2 coupled model simulations, *Clim. Past*, 3, 439-451,  
 457 2007.
- 458 Yanase, W. and Abe-Ouchi, A.: A Numerical Study on the Atmospheric Circulation over the  
 459 Midlatitude North Pacific during the Last Glacial Maximum, *Journal of Climate*, 23, 135-  
 460 151, 2010.
- 461 Yeager, S. G., Shields, C. A., Large, W. G., and Hack, J. J.: The Low-Resolution CCSM3,  
 462 *Journal of Climate*, 19, 2545-2566, 2006.
- 463